Semiclassical molecular dynamics computation of spontaneous light emission in the condensed phase: Resonance Raman spectra

M. Ovchinnikov
Department of Chemistry and Henry Eyring Center for Theoretical Chemistry, 315 South 1400 East Room 2020, University of Utah, Salt Lake City, Utah 84112-0850

V. A. Apkarian
Department of Chemistry, University of California, Irvine, California 92697-2025

Gregory A. Voth
Department of Chemistry and Henry Eyring Center for Theoretical Chemistry, 315 South 1400 East Room 2020, University of Utah, Salt Lake City, Utah 84112-0850

(Received 22 September 2000; accepted 30 January 2001)

The three-time correlation function that describes resonance Raman (RR) spectra is computed directly using the Herman–Kluk semiclassical propagator. The trace expression for this correlation function $\{C(t_1,t_2,t_3)=\mathrm{Tr}[e^{-\beta\hat{H}}e^{-i\hat{H}_g(t_1+t_2)}e^{-i\hat{H}_e t_3}e^{+i\hat{H}_g(t_2+t_3)}e^{+i\hat{H}_e t_1}]\}$ allows forward–backward time propagation of trajectories over closed time-circuits, leading to efficient convergence in multidimensional systems. A local harmonic approximation is used to derive an expression for the density operator in the coherent state representation ($\langle p_1 q_1|e^{-\beta\hat{H}}|p_2 q_2\rangle$). This allows efficient sampling of phase space as well as simulations at arbitrary temperatures and in arbitrary coordinates. The resulting method is first analyzed for a one-dimensional problem, where the results are shown to be in excellent agreement with exact quantum calculations. The method is then applied to the problem of RR scattering of iodine in the condensed phase. The RR spectrum of an I_2 molecule in a xenon fluid at 230 K is calculated and also found to be in excellent agreement with experiment. © *2001 American Institute of Physics.* [DOI: 10.1063/1.1357205]

I. INTRODUCTION

Spectroscopic observables in condensed media, where the density of states is effectively infinite, are more naturally expressed through the time evolution rather than the eigenstates of a system.[1,2] All spectroscopic observables can be computed from quantum time correlation functions.[2] Absorption and emission spectra are expressed through single time correlation functions, while nonlinear (i.e., multiphoton) processes require consideration of correlation functions that depend on multiple time intervals. Although these expressions are rigorous, their evaluation is necessarily approximate, since the core problem of the quantum dynamics of a condensed phase system cannot be solved exactly.

Beginning with the pioneering work of Heller,[1] the use of semiclassical dynamics has been one of the major ways to analyze the spectroscopy of complex systems. The further development of semiclassical initial value representation (SC-IVR) methods[3] that occurred during the last decade has raised hopes that quantities as complex as three-time nonlinear response functions may be computed for nontrivial systems. Indeed, there has been a large volume of work to show that trajectory based SC-IVR methods, and in particular the use of the Herman and Kluk (HK) propagator, are capable of accurately describing quantum dynamics.[4–16] However, once again, the applications have been mostly limited to small systems. The obstacle in this case has been the poor convergence of the methods for sufficiently long times due to the highly oscillatory nature of the phase space integration. The method of forward–backward (FB) propagation, introduced recently, presents the first practical solution to this problem.[17–19]

The application of the FB idea is reasonably straightforward in electronic spectroscopy where the system is propagated on a time-circuit with different (ground or excited state) Hamiltonians as done recently in several works.[16,19] In this work we extend this approach to the calculation of three-time nonlinear response functions for many-body systems at arbitrary temperatures and, as an application, obtain the converged result for the resonance Raman (RR) spectrum of the I_2Xe_{10} 36-dimensional system.

In the next section we describe the physics of spontaneous light emission (SLE) spectroscopy and express the observed signals through the three-time response functions. Section III is devoted to the semiclassical methods. We start by describing the HK semiclassical propagation and its FB implementation for the calculation of linear and nonlinear correlation functions. We then introduce the local harmonic approximation for the density operator, which allows for the efficient evaluation of correlation functions at arbitrary temperature and for the molecular dynamics to be performed in arbitrary coordinates (Cartesian coordinates being the practical choice). The step-by-step execution of the resulting method is described in Sec. IV. In Sec. V we apply this method to compute the resonance Raman correlation functions for a one-dimensional system and compare the results

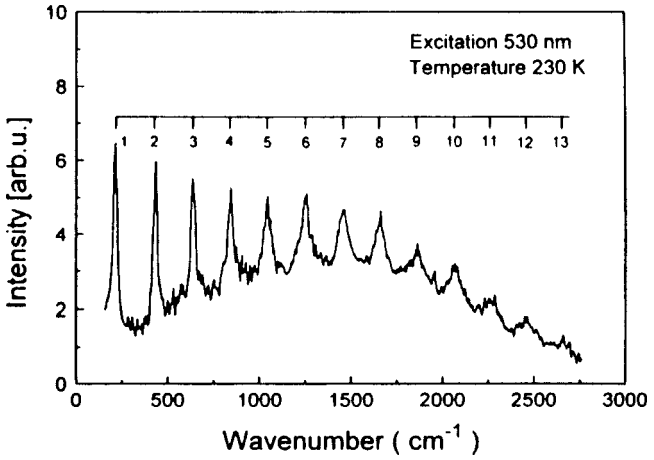

FIG. 1. Experimental SLE spectrum of I_2 in liquid Xe, $\lambda_L = 530$ nm, $T = 230$ K. Reprinted from Ref. 25 with the permission of the authors.

with exact quantum calculations. We show that the spectrum can be analyzed in terms of dynamics of individual trajectories, and we establish the important properties of the three-time correlation functions and its relation to observable spectra. Finally, in Sec. VI we present the results for the condensed phase I_2 in the Xe system and their analysis in terms of molecular dynamics.

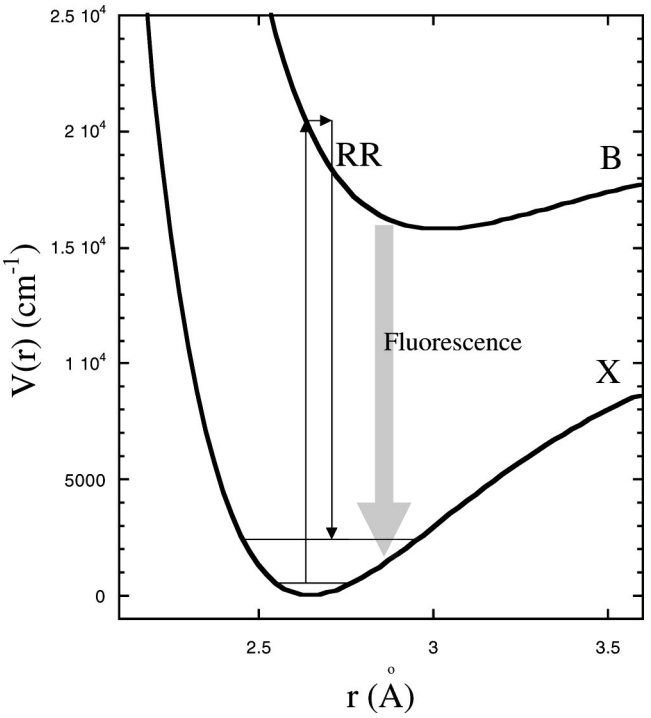

FIG. 2. Schematic representation of the SLE processes, on the I_2 potential energy surfaces.

II. SPONTANEOUS LIGHT EMISSION

It is well recognized that SLE spectra carry rich information about the femtosecond quantum dynamics of a system in its ground and excited electronic states.[2,20–22] The classic example of such experiments are RR and luminescence spectra of I_2 in condensed media. Such experiments on iodine have been carried out in a variety of environments, ranging from solid rare gases at low temperatures to conventional liquids at room temperature.[22–25] The experimental procedure is conceptually simple: one irradiates the sample with laser light at frequency ω_L, and records the spectrum of spontaneous emission $I(\omega_L,\omega_S)$, where ω_S is the frequency of the scattered light. A typical condensed phase measurement [in this case $I(530\text{ nm},\omega_S)$ of iodine in liquid xenon at 230 K] is shown in Fig. 1.[25] The spectrum consists of relatively sharp RR lines, and a broad emission background. The information content in such a measurement can be summarized as follows: (1) Relative intensities of RR overtones I_i and their dependence on the laser frequency ω_L; (2) Broadening and the line shape of the RR overtones which depend strongly on the vibrational mode of the chromophore and the overtone number; and (3) The intensity of the broad luminescence background and its overall shape. While all of these observables are formally expressed through the quantum dynamics of the system, the means of analyzing spectra have been limited, since the calculation of the quantum dynamics of a condensed phase system is so challenging.

The light scattering process is schematically depicted in a plot of the chromophore potential energy surfaces shown in Fig. 2. The relatively sharp progression of RR lines is due to emission during the ballistic evolution of the system on the excited surface, prior to the interaction of the chromophore with its environment. The origin of the broad background is less clear;[26] it is, however, usually assigned to light emitted during the vibrational relaxation of a system on the excited potential energy surface, denoted as ''Fluorescence'' in Fig. 2.

Our calculations are based on the full time dependent interpretation of SLE.[2] Since SLE is a two photon process, it is described by a second order perturbation term with respect to the interaction with the field, which leads to an expression based on three-time nonlinear response correlation functions. For a complete theoretical treatment of the problem we refer the reader to the monograph by Mukamel.[2] The application of this theory to the particular case of I_2 in condensed media is discussed extensively in a recent work by Apkarian and co-workers.[22] For a continuous laser (CW) experiment the SLE spectrum is expressed as a double Fourier transform

$$I(\omega_L,\omega_S) = 2\,\mathrm{Re}\int_0^\infty dt_3\int_0^\infty dt_2\int_0^\infty dt_1 \times[e^{-i\omega_L(t_1+t_2)+i\omega_S(t_2+t_3)}R_3(t_1,t_2,t_3) + e^{-i\omega_L t_1+i\omega_S t_3}R_2(t_1,t_2,t_3) + e^{i\omega_L t_1+i\omega_S t_3}R_1(t_1,t_2,t_3)\,], \quad (1)$$

where the nonlinear response functions are given by

$$R_3(t_1,t_2,t_3) = \mathrm{Tr}[e^{i\hat{H}(t_2+t_3)}\,\hat{\mu}\,e^{i\hat{H}t_1}\,\hat{\mu}\,e^{-\beta\hat{H}} \times e^{-i\hat{H}(t_1+t_2)}\,\hat{\mu}\,e^{-i\hat{H}t_3}\,\hat{\mu}], \quad (2a)$$

$$R_2(t_1,t_2,t_3) = \mathrm{Tr}[e^{i\hat{H}t_3}\,\hat{\mu}\,e^{i\hat{H}(t_1+t_2)}\,\hat{\mu}\,e^{-\beta\hat{H}} \times e^{-i\hat{H}t_1}\,\hat{\mu}\,e^{-i\hat{H}(t_2+t_3)}\,\hat{\mu}], \quad (2b)$$

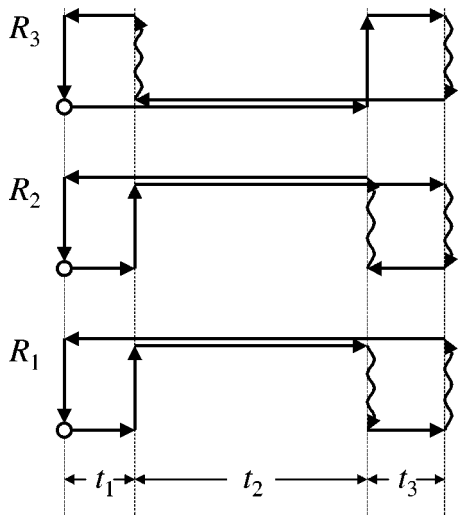

FIG. 3. The time-circuit diagrams which represent the nonlinear response functions in Eqs. (4).

$$R_1(t_1,t_2,t_3)=\mathrm{Tr}[\hat{\mu}\, e^{i\hat{H}(t_1+t_2+t_3)}\,\hat{\mu}\, e^{-\beta\hat{H}} \times e^{-i\hat{H}t_1}\,\hat{\mu}\, e^{-i\hat{H}t_2}\,\hat{\mu}\, e^{-i\hat{H}t_3}]. \tag{2c}$$

(Here and throughout the paper we use atomic units in which $\hbar=1$.)

When the laser frequency corresponds to a transition between two electronic states of the system, the dipole moment acts as an operator that transfers the wave function between the electronic surfaces. We use the commonly made Condon approximation (i.e., that the transition dipole moment does not depend on the position of the nuclei) so the dipole operator can be written simply as a matrix

$$\hat{\mu}=\begin{pmatrix} 0 & \mu_{12} \\ \mu_{12} & 0 \end{pmatrix}. \tag{3}$$

The response functions in Eqs. (2) are then given as a trace of the density matrix propagated sequentially on the ground and excited electronic states. Using the cyclic permutation rule for the trace, and omitting the constant factor of μ_{12}^4, we can rewrite the response functions as

$$R_3(t_1,t_2,t_3)=\mathrm{Tr}[\, e^{-\beta\hat{H}_g}\, e^{-i\hat{H}_g(t_1+t_2)} \times e^{-i\hat{H}_e t_3}\, e^{i\hat{H}_g(t_2+t_3)}\, e^{i\hat{H}_e t_1}\,], \tag{4a}$$

$$R_2(t_1,t_2,t_3)=\mathrm{Tr}[\, e^{-\beta\hat{H}_g}\, e^{-i\hat{H}_g t_1}\, e^{-i\hat{H}_e(t_2+t_3)} \times e^{i\hat{H}_g t_3}\, e^{i\hat{H}_e(t_1+t_2)}\,], \tag{4b}$$

$$R_1(t_1,t_2,t_3)=\mathrm{Tr}[\, e^{-\beta\hat{H}_g}\, e^{-i\hat{H}_g t_1}\, e^{-i\hat{H}_e t_2} \times e^{-i\hat{H}_g t_3}\, e^{i\hat{H}_e(t_1+t_2+t_3)}\,]. \tag{4c}$$

A useful way to interpret the above expressions is to represent them with the Feynman-type time-circuit diagrams shown in Fig. 3. Here the lower lines correspond to propagation on the ground potential surface and the upper lines on the excited surface. The ends of the circuit are connected via the density operator $e^{-\beta\hat{H}_g}$ represented by a circle. The three diagrams have important features in common. For the time intervals t_1 and t_3, the propagation of the density is done on different electronic surfaces forward and backward in time (in the language of Liouvillian dynamics this is called propagation of the coherence of the density matrix). This leads to the fact that in many condensed phase systems the correlation functions in Eqs. (4) are nonzero only for the short time intervals t_1 and t_3 due to rapid electronic dephasing. For the time interval t_2, backward and forward propagation happens on the same potential energy surface (i.e., the electronic population of the density is propagated); thus the correlation function survives for an arbitrarily long time t_2, provided that t_1 and t_3 are sufficiently short. Indeed, for the limiting case of $t_1=t_3=0$, all of the correlation functions Eqs. (4) are unity: $R(0,t_2,0)\equiv 1$. The R_3 correlation function [Eq. (4a)] carries long time dynamics on the ground state and is therefore responsible for the sharp RR structure. Similarly, Eqs. (4b) and (4c) include long time propagation on the excited state. However, the Fourier expression in Eq. (1) does not include any frequency filtering in time t_2, which results in the absence of any vibrational structure in the fluorescence signal.

As far as we know, the correlation functions in Eqs. (4) have never been explicitly evaluated even for small systems. For model systems such as the multi-mode harmonic oscillator and Brownian oscillator model, components of the SLE spectrum in Eq. (1) were obtained in the frequency domain analytically.[2] A limited treatment of RR spectra in the condensed phase has also been possible using the time dependent self consistent field (TDSCF) (Ref. 27) method and mixed-order semiclassical dynamics.[28] In these works, a partially time dependent formulation has been used to compute the intensities of the RR overtones. If one assumes that the ground state vibrational eigenstates are known, one can rewrite the contribution of R_3 to the overall spectrum in Eq. (1) at $T=0$:

$$I_{\mathrm{Raman}}(\omega_L,\omega_S)=\sum_i \delta(\omega_L-\omega_S-E_i) \times\left|\int_0^\infty dt\, e^{i\omega_L t}\langle\psi_i|\, e^{-i\hat{H}_e t}|\psi_0\rangle\right|^2, \tag{5}$$

where the summation is carried out over all vibrational states i of the ground state potential surface. Originally formulated by Heller and co-workers,[20] this treatment has been the primary tool for the analysis of RR spectra. This method can only be applied to the condensed phase under the assumption that solute and solvent dynamics in the ground electronic state can be completely separated. Thus this treatment simply avoids the issue of the dynamics on the ground state and addresses only the first property measured in the experiment (i.e., the relative intensities of RR overtones), while the information about their line shapes as well as the luminescence background is lost. The opposite approach, also widely known but suitable only for the off-resonance Raman spectrum, is to neglect dynamics on the excited state and to consider only the dynamics on the ground state.[29] In this limit the integrals over t_1 and t_3 in Eq. (1) are replaced by the polarizability operators leading to the expression

$$I_{\mathrm{Raman}}(\omega_L,\omega_S)\sim \mathrm{Re}\int_0^\infty dt\, e^{i(\omega_L-\omega_S)t}\langle\hat{\alpha}(0)\hat{\alpha}(t)\rangle. \tag{6}$$

Both approximations Eqs. (5) and (6) neglect part of the physics essential for a complete understanding of SLE.

In this paper we apply the semiclassical methods described in the next section toward the calculation of the SLE spectra. We limit the present treatment, however, to the calculation of the RR correlation function R_3. Consideration of the fluorescence contributions, R_1 and R_2, requires only minor modifications of the methodology and we plan to perform these calculations in the subsequent work. A strictly classical treatment of R_1 and R_2 contributions can be found in Ref. 22.

III. THEORETICAL METHODS

A. Herman–Kluk propagator

The HK propagator has been the subject of numerous studies.[4,5,7,8,10–15,30] Here we identify the main concepts that are important for the present development. The starting point is the expression of the quantum propagator as a sum over classical trajectories,[4]

$$e^{-i\hat{H}t}=\int d^N\mathbf{p}_0\, d^N\mathbf{q}_0\, J_{\mathbf{p}_0,\mathbf{q}_0,t}\, e^{i\,S_{\mathbf{p}_0,\mathbf{q}_0,t}}\,|\mathbf{p}_t,\mathbf{q}_t\rangle\langle\mathbf{p}_0,\mathbf{q}_0|, \tag{7}$$

where we define coherent states as

$$\langle\mathbf{x}|\mathbf{p},\mathbf{q}\rangle=\left(\frac{\det\boldsymbol{\gamma}}{\pi^N}\right)^{1/4} e^{1/2(\mathbf{x}-\mathbf{q})\,\gamma(\mathbf{x}-\mathbf{q})\,+\,i\mathbf{p}\,(\mathbf{x}-\mathbf{q})}. \tag{8}$$

In general, the width parameter γ can be an arbitrary positive definite matrix. However, the usual choice of γ is a matrix that is diagonal in the coordinates in which the classical dynamics is evaluated. $S_{\mathbf{p}_0,\mathbf{q}_0,t}$ is the classical action at time t of a trajectory originating at $\mathbf{p}_0,\mathbf{q}_0$. The pre-exponential factor $J_{\mathbf{p},\mathbf{q},t}$ is expressed through blocks of the monodromy matrix as

$$J_{\mathbf{p}_0,\mathbf{q}_0,t}=\left(\det\left[\frac{1}{2}\left(\gamma^{1/2}\frac{\partial\mathbf{q}_t}{\partial\mathbf{q}_0}\gamma^{-1/2}+\gamma^{-1/2}\frac{\partial\mathbf{p}_t}{\partial\mathbf{p}_0}\gamma^{1/2}-i\,\gamma^{1/2}\frac{\partial\mathbf{q}_t}{\partial\mathbf{p}_0}\gamma^{1/2}+i\,\gamma^{-1/2}\frac{\partial\mathbf{p}_t}{\partial\mathbf{q}_0}\gamma^{-1/2}\right)\right]\right)^{1/2}. \tag{9}$$

The matrices $\partial\mathbf{q}_t/\partial\mathbf{q}_0$, $\partial\mathbf{p}_t/\partial\mathbf{p}_0$, $\partial\mathbf{q}_t/\partial\mathbf{p}_0$, $\partial\mathbf{p}_t/\partial\mathbf{q}_0$ in the above equation are obtained by integrating auxiliary equations, which are similar to the Hamilton equations of motion.[4,5,7] Instead of $2N$ independent variables of simple Hamiltonian dynamics, the dynamics is carried out for $2N+4N^2+1$ variables, which leads to an N^3 type scaling for each individual trajectory. It is not, however, this scaling that has limited the application of the method so far. With present computer capabilities such dynamics can be evaluated for systems where N is of the order of 100. The main problem with realistic applications has been the slow convergence of the phase space integration in Eq. (7). Consider the application of Eq. (7) to calculate an arbitrary correlation function of the form

$$\langle\Psi_2|e^{-i\hat{H}t}|\Psi_1\rangle=\int d^N\mathbf{p}_0\, d^N\mathbf{q}_0\, J_{\mathbf{p}_0,\mathbf{q}_0,t}\, e^{i\,S_{\mathbf{p}_0,\mathbf{q}_0,t}}\times\langle\Psi_2|\mathbf{p}_t,\mathbf{q}_t\rangle\langle\mathbf{p}_0,\mathbf{q}_0|\Psi_1\rangle. \tag{10}$$

The phase space integration is usually accomplished by sampling an ensemble of phase space points $\{\mathbf{p}_{0i},\mathbf{q}_{0i}\}$ from some distribution $\rho(\mathbf{p}_0,\mathbf{q}_0)$ using the Monte Carlo (MC) method. Sensible choices for this distribution are $\rho(\mathbf{p}_0,\mathbf{q}_0)=\langle\mathbf{p}_0,\mathbf{q}_0|\Psi_1\rangle$ or $\rho(\mathbf{p}_0,\mathbf{q}_0)=\langle\Psi_2|\mathbf{p}_0,\mathbf{q}_0\rangle\langle\mathbf{p}_0,\mathbf{q}_0|\Psi_1\rangle$. The correlation function is evaluated as

$$\langle\Psi_2|e^{-i\hat{H}t}|\Psi_1\rangle=\frac{1}{n}\sum_{i=1}^{n}\rho^{-1}(\mathbf{p}_{0i},\mathbf{q}_{0i})\,J_{ti}e^{i\,S_{\mathbf{ti}}}\times\langle\Psi_2|\mathbf{p}_{ti},\mathbf{q}_{ti}\rangle\langle\mathbf{p}_{0i},\mathbf{q}_{0i}|\Psi_1\rangle. \tag{11}$$

The standard statistical deviation of the right hand side of this equation can be estimated as $A_t n^{-1/2}$, where $A_t\sim\langle|J_t|\rangle$ is the average absolute value of the integrand in Eq. (11).[31] For a general nonlinear dynamics the pre-exponential factor J_t increases exponentially with time t, $\langle|J_t|\rangle\sim\exp(\mathrm{const}\,Nt)$. This leads to effectively an exponential scaling of the method with the number of degrees of freedom N. The FB method, however, presents an elegant solution to this problem.[17–19]

B. Application of the FB propagation

It is recognized that a large number of observables can be expressed through correlation functions of the form

$$C(t)=\mathrm{Tr}[e^{-\beta\hat{H}}\hat{A}\,e^{i\hat{H}t}\hat{B}\,e^{-i\hat{H}t}], \tag{12}$$

which includes propagators both forward and backward in time.[17] The main idea of the FB method is to combine these two operators as a single semiclassical expression such as Eq. (7). Indeed, if a trajectory is propagated with the Hamiltonian H for time t and for time $-t$ (or equivalently forward in time with the Hamiltonian $-H$) it arrives back at the initial point due to reversibility of classical mechanics: $|p_{+t-t},q_{+t-t}\rangle=|\mathbf{p}_0,\mathbf{q}_0\rangle$. Similarly the prefactor reduces back to its original value $J_{+t-t}=1$. Of course, any meaningful correlation function would have an operator $\hat{B}$ between forward and backward propagation. The essence of the method worked out by Miller and co-workers[18] is the incorporation of an arbitrary operator $\hat{B}$ into a semiclassical FB propagator. In this case the backward trajectories do not exactly cancel the forward ones. However, it was shown that if the effect of $\hat{B}$ is small, there is a significant cancellation between forward and backward trajectories resulting in a relatively small absolute values of J so that Eq. (7) can be more readily converged by MC.

The FB idea is easily extended for the calculation of correlation functions that arise in electronic spectroscopy, where difference in forward and backward trajectories results from propagation on different potential energy surfaces. The linear response (electronic absorption) correlation function is then given by[19]

$$C(t)=\mathrm{Tr}[e^{-\beta\hat{H}_g}e^{-i\hat{H}_e t}\,e^{i\hat{H}_g t}]$$
$$=\int d^N\mathbf{p}_0\,d^N\mathbf{q}_0\,\{\langle\mathbf{p}_{+t-t},\mathbf{q}_{+t-t}|e^{-\beta\hat{H}_g}|\mathbf{p}_0,\mathbf{q}_0\rangle \times J_{\mathbf{p}_0,\mathbf{q}_0,+t-t}\,e^{iS_{\mathbf{p}_0,\mathbf{q}_0,+t-t}}\}, \tag{13}$$

where $\hat{H}_g$ and $\hat{H}_e$ are the Hamiltonians of the ground and excited electronic states, respectively. The end point of a trajectory is obtained by integrating the equations of motion with the H_e for time t and then with H_g for time $-t$. Similarly, we can express any of the two-photon response functions Eqs. (4) as

$$R_i(t_1,t_2,t_3)=\int d^N\mathbf{p}_0\,d^N\mathbf{q}_0 \times\{\langle\mathbf{p}_{t_1,t_2,t_3},\mathbf{q}_{t_1,t_2,t_3}|e^{-\beta\hat{H}_g}|\mathbf{p}_0,\mathbf{q}_0\rangle \times J_{\mathbf{p}_0,\mathbf{q}_0,t_1,t_2,t_3}e^{iS_{\mathbf{p}_0,\mathbf{q}_0,t_1,t_2,t_3}}\}, \tag{14}$$

where the final phase space point is the result of classical propagation on a time-circuit with a series of Hamiltonians that switch from ground to excited state as specified by the diagrams shown in Fig. 3.

If the ground and excited state Hamiltonians are significantly different, there is little point in propagating trajectories forward and backward to evaluate the linear correlation function Eq. (13) since there would be minimal cancellation. However, in a number of condensed phase problems the ground and excited states are different only in few degrees of freedom which correspond to the chromophore and maybe a few of the solvent modes coupled to the electronic transition. Thus, by doing FB propagation in Eq. (13) one effectively cancels the effect of the nonlinear dynamics of the solvent that is not directly coupled to the chromophore transition. Moreover, as it is shown in the next subsection the coherent state density matrix element $\langle\mathbf{p}_1,\mathbf{q}_1|e^{-\beta\hat{H}_g}|\mathbf{p}_2,\mathbf{q}_2\rangle$ is well represented under certain conditions by a Gaussian in the position and momentum difference of the phase space points $(\mathbf{p}_1,\mathbf{q}_1)$ and $(\mathbf{p}_2,\mathbf{q}_2)$. Therefore the contribution of trajectory to the correlation function rapidly becomes zero if its initial and final phase space points differ in many dimensions. The combined effect of these two considerations is what makes the method practical for many-dimensional problems: If there is FB cancellation at least in most of the degrees of freedom, the pre-exponential factor J stays small and if the separation between initial and final phase space points is large the contribution of the trajectory becomes negligible due to the rapid decay of the thermal density matrix element. For the nonlinear response correlation functions such as Eqs. (4) considered in this work, the loop in time is particularly important, since the trajectory runs on different surfaces only for the short time intervals t_1 and t_3 and remains on the same surface for a longer time t_2.

The only component that is missing so far to make the method practical is a way to efficiently evaluate the density operator matrix element in the coherent state representation. The next subsection is devoted to this subject.

C. Local harmonic approximation for the density operator

We start by writing the density operator as a path integral expression[32]

$$\langle\mathbf{p}_1,\mathbf{q}_1|e^{-\beta\hat{H}}|\mathbf{p}_2,\mathbf{q}_2\rangle = \int d\mathbf{x}_1\,d\mathbf{x}_2\,\langle\mathbf{p}_1,\mathbf{q}_1|\mathbf{x}_1\rangle\int_{\tau=0,\mathbf{x}=\mathbf{x}_1}^{\tau=\beta,\mathbf{x}=\mathbf{x}_2}\mathcal{D}[\mathbf{x}(t)]\,e^{-\int H d\tau} \times\langle\mathbf{x}_2|\mathbf{p}_2,\mathbf{q}_2\rangle. \tag{15}$$

While this expression can be evaluated directly using imaginary time path integral methods, here we seek a more approximate and efficient solution. We assume that the points $(\mathbf{p}_1,\ \mathbf{q}_1)$ and $(\mathbf{p}_2,\ \mathbf{q}_2)$ are sufficiently close that the overlap $\langle\mathbf{p}_1,\mathbf{q}_1|\mathbf{p}_2,\mathbf{q}_2\rangle$ is significant. At sufficiently high temperature the integration paths in Eq. (15) will be short and they will not sample the potential in regions far from points $\mathbf{q}_1$ and $\mathbf{q}_2$. It is natural then to use the local harmonic approximation for the Hamiltonian in Eq. (15), i.e., to expand the potential energy in a Taylor series around a given point $\mathbf{q}_0$ that lies in the proximity of the points $\mathbf{q}_1$ and $\mathbf{q}_2$,

$$V(\mathbf{x})\approx V(\mathbf{q}_0)+V'(\mathbf{q}_0)(\mathbf{x}-\mathbf{q}_0) +\tfrac{1}{2}(\mathbf{x}-\mathbf{q}_0)\,V''(\mathbf{q}_0)\,(\mathbf{x}-\mathbf{q}_0), \tag{16}$$

where in a general N-dimensional case V' is a vector and V'' is an $N\times N$ matrix. At sufficiently high temperature this approximation is of similar order as the semiclassical dynamics itself, since the HK propagator assumes that the potential is locally quadratic over the width of coherent state Gaussians. Using expression in Eq. (16) the path integral in Eq. (15) can be evaluated analytically, and we use the known expression for the harmonic oscillator density matrix in coordinate representation[32] to obtain an expression convenient for analytical integration

$$\langle\tilde{\mathbf{x}}-\Delta\mathbf{x}/2|\,e^{-\beta\hat{H}}|\tilde{\mathbf{x}}+\Delta\mathbf{x}/2\rangle\approx\exp[-\beta V_0-\tfrac{1}{4}\Delta\mathbf{x}\,\alpha\,\Delta\mathbf{x} -\tfrac{1}{4}(\tilde{\mathbf{x}}-\mathbf{x}_0)\,\sigma\,(\tilde{\mathbf{x}}-\mathbf{x}_0)]. \tag{17}$$

Here, we changed the variables to $\Delta\mathbf{x}=\mathbf{x}_2-\mathbf{x}_1$ and $\tilde{\mathbf{x}}=(\mathbf{x}_2+\mathbf{x}_1)/2$, and $\mathbf{x}_0$ and V_0 denote the position and the potential energy of the minimum of the harmonic expansion in Eq. (16). These quantities are given by the simple relations

$$\mathbf{x}_0=\mathbf{q}_0-V''^{-1}V', \tag{18}$$

$$V_0=V(\mathbf{q}_0)-\tfrac{1}{2}(\mathbf{q}_0-V''^{-1}V')\,V''\,(\mathbf{q}_0-V''^{-1}V'). \tag{19}$$

The $N\times N$ matrices α and σ are diagonal in the local normal modes and their elements are given by the expressions

$$\alpha_{ii}^{(0)}=m_i\omega_i\frac{\cosh(\beta\omega_i)+1}{\sinh(\beta\omega_i)}, \tag{20}$$

$$\sigma_{ii}^{(0)}=m_i\omega_i\frac{\cosh(\beta\omega_i)-1}{\sinh(\beta\omega_i)}, \tag{21}$$

where the superscript (0) indicates that these are the values for the normal mode coordinates, ω_i being the normal fre-

quencies of the system. In an arbitrary coordinate system the matrices α and σ are obtained using the standard coordinate transformation.

After we substitute the density matrix approximation Eq. (17), Eq. (15) becomes a Gaussian integral. The actual integration is simplest if we use $\Delta\mathbf{x}$ and $\tilde{\mathbf{x}}$ as integration variables instead of the $\mathbf{x}_1$, $\mathbf{x}_2$, and leads to the following result:

$$\begin{aligned}\langle \mathbf{p}_1,\mathbf{q}_1|e^{-\beta\hat{H}}|\mathbf{p}_2,\mathbf{q}_2\rangle &\approx \exp[-(\tilde{\mathbf{q}}-\mathbf{x}_0)\,\sigma\,\gamma\,(\sigma+\gamma)^{-1}(\tilde{\mathbf{q}}-\mathbf{x}_0) \\ &\quad -\tilde{\mathbf{p}}\,(\alpha+\gamma)^{-1}\tilde{\mathbf{p}}-\beta V_0\,] \\ &\quad \times\exp[-\tfrac{1}{4}\Delta\mathbf{q}\,\alpha\,\gamma\,(\alpha+\gamma)^{-1}\Delta\mathbf{q} \\ &\quad -\tfrac{1}{4}\Delta\mathbf{p}\,(\sigma+\gamma)^{-1}\Delta\mathbf{p}] \\ &\quad \times\exp[\,i\,\tilde{\mathbf{p}}\,\alpha\,(\gamma+\alpha)^{-1}\,\Delta\mathbf{q}-i\,\tilde{\mathbf{q}}\,\sigma\,(\sigma+\gamma)^{-1}\,\Delta\mathbf{p}\,],\end{aligned} \tag{22}$$

where we have defined the vectors $\tilde{\mathbf{q}}=(\mathbf{q}_1+\mathbf{q}_2)/2$, $\tilde{\mathbf{p}}=(\mathbf{p}_1+\mathbf{p}_2)/2$, $\Delta\mathbf{q}=\mathbf{q}_2-\mathbf{q}_1$, and $\Delta\mathbf{p}=\mathbf{p}_2-\mathbf{p}_1$.

Equation (22) is written as a product of three exponential factors. When the phase space points $(\mathbf{q}_1,\mathbf{p}_1)$ and $(\mathbf{q}_2,\mathbf{p}_2)$ coincide, $\Delta\mathbf{q}=\Delta\mathbf{p}=0$, and the second and third factors in Eq. (22) vanish. We are then left with the first term that gives a local harmonic approximation to the Husimi distribution $\langle\tilde{\mathbf{p}},\tilde{\mathbf{q}}|e^{-\beta\hat{H}}|\tilde{\mathbf{p}},\tilde{\mathbf{q}}\rangle$. The second term in this expression is Gaussian in the differences $\Delta\mathbf{q}$ and $\Delta\mathbf{p}$. The higher the temperature the narrower is the width of this Gaussian. The high temperature limit of the overall expression is obtained by keeping the leading order terms in Eqs. (20) and (21) to obtain

$$\beta\to 0:\quad \alpha_{ii}^{(0)}\approx 2\beta^{-1}m_i\gg\boldsymbol{\gamma}_{ii},\quad \sigma_{ii}^{(0)}\approx\tfrac{1}{2}\beta m_i\omega_i^2\ll\boldsymbol{\gamma}_{ii}. \tag{23}$$

Taking the appropriate limits for the coefficients in Eq. (22) one notices that the first line reduces to a simple Boltzmann distribution, while the second and third line combine into the overlap of coherent states leading to a ''local'' approximation for the density operator

$$\beta\to 0:\langle \mathbf{p}_1,\mathbf{q}_1|e^{-\beta\hat{H}}|\mathbf{p}_2,\mathbf{q}_2\rangle\approx e^{-\beta H(\tilde{\mathbf{p}},\tilde{\mathbf{q}})}\langle \mathbf{p}_1,\mathbf{q}_1|\mathbf{p}_2,\mathbf{q}_2\rangle. \tag{24}$$

Expression (22) is exact for any harmonic system. For anharmonic systems the approximation is valid when the paths in the exact expression in Eq. (15) do not sample the region far away from the points $\mathbf{q}_1$ and $\mathbf{q}_2$ and the latter two points are not far apart. As a reasonable criterion, one might require that the typical displacement of the integration path in Eq. (15) is within the width of the coherent state $\boldsymbol{\gamma}^{-1/2}$ which restricts the temperature to $kT\gtrsim\boldsymbol{\gamma}$, i.e., the temperature is greater or comparable to the uncertainty energy of a coherent state. However, at lower temperatures, a typical condensed phase system is solid and is described quite well by the harmonic approximation. This may validate the use of the approximation over a broad range of temperatures.

It should also be noted that the expression in Eq. (22) allows for the possibility of the imaginary frequencies and thus complex matrices α and σ. However, for the particular system considered in this work the approximation of the imaginary frequencies in Eqs. (20) and (21) by zero was found to be sufficiently accurate.

Let us now consider the incorporation of the Eq. (22) within the FB method for the calculation of the correlation functions in Eqs. (13) and (14). To evaluate these expressions, we first sample the initial conditions $\mathbf{p}_0,\mathbf{q}_0$ by MC. The natural sampling function is given by the Husimi distribution since that ensures the same contribution of each trajectory to the response function at $t_1=t_2=t_3=0$. After the point has been sampled we need to propagate many classical trajectories on the loops specified by given time intervals and correlate the end points with the initial point using Eq. (22). The calculation of the local harmonic approximation to the potential is computationally expensive, since it requires diagonalization of the Hessian V''. Fortunately we can avoid doing this operation after each time loop by making an expansion of the potential around the single initial point of all trajectories $\mathbf{q}_0$. Thus prior to any dynamics we find the normal modes of potential at the origin of trajectories and precompute all parameters in Eq. (22). The vectors and matrices are stored in memory until we are done with these initial conditions to allow the efficient evaluation of Eq. (22). Note that the matrix form of Eq. (22) is valid in any coordinate system, which allows us to perform semiclassical dynamics in arbitrary coordinates.

It is interesting to examine the application of this method to a system–bath-like Hamiltonian such as in the I_2/Xe problem we consider later. Consider the Hamiltonians

$$H_g=H_{(s)g}+H_{(b)}+H_{(sb)},\quad H_e=H_{(s)e}+H_{(b)}+H_{(sb)}, \tag{25}$$

where the only part that differs from ground to excited state is the system Hamiltonians $H_{(s)g}$ and $H_{(s)e}$; the bath Hamiltonian $H_{(b)}$ and the system–bath interaction $H_{(sb)}$ are the same for both electronic states. If there is no system–bath interaction $[H_{(sb)}=0]$, the propagation of the bath degrees of freedom cancels exactly, so that aside from carrying the dynamics for bath degrees of freedom, our results are numerically identical to those for the isolated system. If we introduce the system–bath interaction, the backward trajectory is formally displaced from the forward one in all degrees of freedom. This many-dimensional displacement of the final point from the initial one has two effects: the first is the growth of the preexponential factor J, while the second is the decay of the matrix element $\langle \mathbf{p}_0,\mathbf{q}_0|e^{-\beta\hat{H}}|\mathbf{p}_f,\mathbf{q}_f\rangle$. Note that if the initial and final points are slightly misplaced in all bath degrees of freedom, the sheer number of the bath coordinates makes the overlap close to zero. Hence, it will be the competition between these two processes which determines how readily the MC approximation to Eq. (14) converges. This issue of prefactor growth vs matrix element decay is very important in the overall convergence of the method especially in many dimensional systems and should perhaps be investigated in a more formal manner. In this work, however, we have found that this relationship is in our favor and the method converges very efficiently due to a fast decay of the thermal density matrix element.

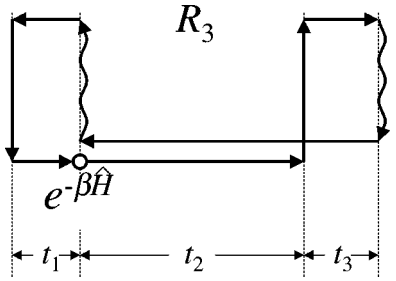

FIG. 4. The time-circuit diagram which represents the propagation scheme for the semiclassical evaluation of the response function R_3.

A conceptually simplified method to evaluate the correlation functions arises if we use the high temperature ''local'' approximation for the density matrix in Eq. (24). In this case the Husimi distribution reduces to a simple Boltzmann distribution, which can be sampled by ordinary MC, and the coherent state density matrix Eq. (24) can be simply evaluated within the code. This simplified method leads to a numerical procedure very similar to the method that was proposed previously without giving a rigorous derivation.[28] In a recent paper by Kuhn and Makri,[19] where the absorption spectrum of iodine in a one dimensional chain of argon atoms is considered, this approximation has been used for the bath degrees of freedom, while for the I_2 vibrational degree of freedom the density matrix has been constructed from the ground vibrational state. While such an approximation works reasonably well for this problem,[28] its drawback is the necessity to carry out the dynamics in a coordinate system that separates out the I_2 vibrational degree of freedom. In our present formulation, the computation can be done directly in the Cartesian coordinates of the atoms.

IV. NUMERICAL IMPLEMENTATION

Here we provide a step-by-step description of the numerical procedure used to compute the nonlinear response function in Eq. (4a). This procedure is as follows:

(1) The Metropolis MC algorithm is used to sample the initial conditions $(\mathbf{p}_0, \mathbf{q}_0)$ from the Husimi distribution. Equation (22) is used to evaluate the Husimi distribution, in which the local normal modes as well as the matrices $\boldsymbol{\alpha}$ and σ are recalculated for every accepted step of the MC. After acceptance of initial conditions the local normal modes are redetermined, the matrices α, σ, as well as parameters $\mathbf{x}_0$ and V_0 are first computed using the expressions in Eq. (20) and (21) in the local normal mode coordinate system, and then converted to Cartesian coordinates. All the matrices that enter Eq. (22), i.e., $\sigma\gamma(\sigma+\gamma)^{-1}$, $(\alpha+\gamma)^{-1}$, $\alpha\gamma(\alpha+\gamma)^{-1}$, $(\sigma+\gamma)^{-1}$, $\alpha(\gamma+\alpha)^{-1}$, and $\sigma(\sigma+\gamma)^{-1}$, are computed and stored in memory.

(2) Trajectories are propagated on the time-circuits specified by the intervals t_1, t_2, t_3. The time-circuit propagation is rewritten in the following order:

$$R_3(t_1,t_2,t_3)=[\, e^{-\beta\hat{H}_g}\, e^{-i\hat{H}_g t_2}\, e^{-i\hat{H}_e t_3}\, e^{i\hat{H}_g t_3} \times e^{i\hat{H}_g t_2}\, e^{i\hat{H}_e t_1}\, e^{-i\hat{H}_g t_1}], \tag{26}$$

which is represented by a slightly different time-circuit diagram shown in Fig. 4. This is possible since the propagator on the ground state Hamiltonian $e^{-i\hat{H}_g t}$ commutes with the density operator $e^{-\beta\hat{H}_g}$. This ordering has the numerical advantage of separating the propagation along the t_2–t_3 plane from the t_1 interval.

(3) At the end of each time-circuit the final phase space point is correlated with the initial one using Eq. (22) with the matrices precomputed from step (1). We add the contribution of a trajectory as given by Eq. (14) to the total correlation function.

(4) For a given set of initial conditions, the propagation is repeated for all grid points along the three time axes.

(5) Steps (1)–(4) are repeated until convergence of the phase space integral Eq. (14) is reached.

The classical propagation forward in time is obtained with the first order symplectic steps

$$\mathbf{p}(t+dt)=\mathbf{p}(t)-V'(\mathbf{q}(t))\,dt;$$
$$\mathbf{q}(t+dt)=\mathbf{q}(t)+\mathbf{p}(t+dt)/m\,dt; \tag{27}$$

and the backward propagation is done by the steps

$$\mathbf{q}(t-dt)=\mathbf{q}(t)-\mathbf{p}(t)/m\,dt;$$
$$\mathbf{p}(t-dt)=\mathbf{p}(t)+V'(\mathbf{q}(t-dt))\,dt. \tag{28}$$

Similar expressions are used to compute the dynamics of the monodromy matrix. Note that while the accuracy of the first order integrator is only $O(dt^2)$, complete numerical reversibility of forward and backward propagation is satisfied. This turns out to be crucial for the successful application of the method to many-body nonlinear systems where the numerical divergence of forward and backward propagation due to integrator error could lead to a substantial loss of the correlation.

V. ONE-DIMENSIONAL SYSTEM

In this section the Raman three-time correlation function $R_3(t_1,t_2,t_3)$ is calculated for a one-dimensional system. The problem of choice is an isolated I_2 molecule represented by two electronic states. The potentials of the ground X and excited B electronic states are given by the Morse functions used previously,[28] which are shown in Fig. 2. The correlation function is computed on a three-dimensional time grid $t_1,t_3=0,1,\ldots,25$ fs, $t_2=0,5,10,\ldots,3000$ fs. The choice of time intervals and step sizes is motivated by the physics of the problem. A duration of 3000 fs for t_2 determines the resolution of the Raman spectral lines, the time step of $\Delta t_2=5$ fs is a lower limit to obtain the spectrum in a sufficiently wide spectral range $\omega_{\max}=2\pi/\Delta t_2=6700\ \mathrm{cm}^{-1}$. The intervals t_1 and t_3 are chosen with the condensed phase application in mind: 25 fs resolves the initial decay of the correlation function due to the rapid motion of the wave packet on the repulsive wall of the B state. In the condensed phase these time intervals are sufficient, since after the initial decay the correlation remains zero. In the one-dimensional problem restriction of the times simply makes the potential of the B state effectively dissociative (i.e., the vibrational spectrum of state B is artificially taken to be continuous).

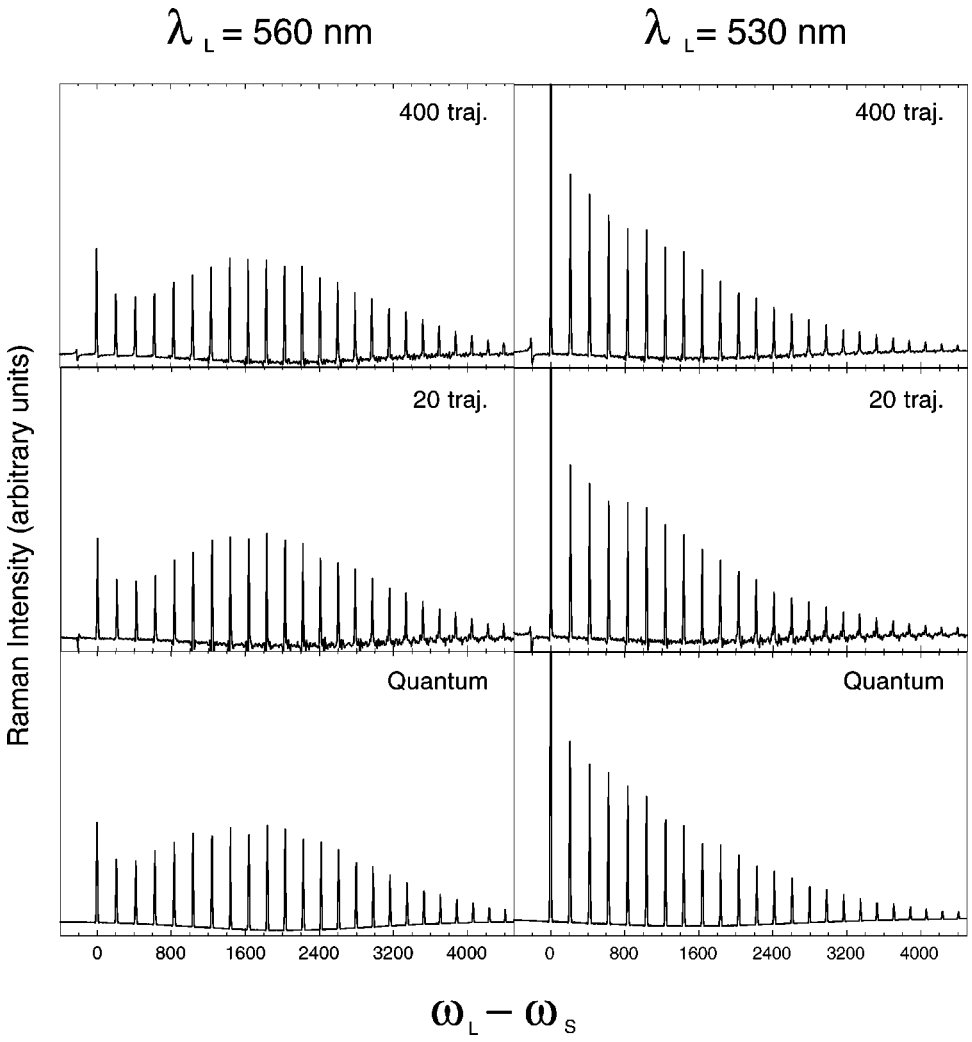

FIG. 5. Resonance Raman spectra of the one dimensional system at $T=0$ (see text). (Top panels) 400 phase space initial condition semiclassical calculation; (middle panels) 20 phase space initial condition semiclassical calculation; (bottom panels) exact quantum mechanical results.

In one dimension we compare the semiclassical calculations to the results of the exact quantum calculations. The quantum response functions are constructed on the same grid in t_1,t_2,t_3 space by using the vibrational eigenstate representation of quantum propagators

$$R_3(t_1,t_2,t_3)=\sum_{i,j,\mu,\nu} e^{-\beta E_i}e^{-iE_i(t_1+t_2)}e^{-iE_\mu t_3} \times e^{iE_j(t_2+t_3)}e^{iE_\nu t_1}\langle i|\mu\rangle\langle\mu|j\rangle\langle j|\nu\rangle\langle\nu|i\rangle, \tag{29}$$

where the Roman indices i, j enumerate the vibrational eigenstates of the X potential and the Greek indices μ and ν are the states of the B surface. The energies and the Frank-Condon factors of the vibrational states are computed using the standard DVR method.[33] It should be noted that, although the procedure is straightforward, it is significantly less efficient than the semiclassical dynamics due to the very large number of summations in Eq. (29).

Since the X state potential is described extremely well as a harmonic oscillator in the region around its minimum, the local harmonic approximation for the density matrix is valid at all temperatures. We first compute the response function and the spectra for the $T=0$ case. The RR spectra shown in Fig. 5 are obtained by taking the double Fourier transform of the response functions. A Gaussian window function is applied in order to smooth the oscillations in the spectral lines that occur due to the ''box'' integration. The spectra are given by

$$I_{\text{Raman}}(\omega_L,\omega_S)=2\,\text{Re}\int_0^\infty dt_3\int_0^\infty dt_2\int_0^\infty dt_1 e^{-(t_2/t_w)^2} \times e^{-i\omega_L(t_1+t_2)+i\omega_S(t_2+t_3)}R_3(t_1,t_2,t_3) \tag{30}$$

at the laser frequency of $\omega_L=2\pi c/\lambda_L$ and window parameter $t_w=1600$ fs. The results of the 400 initial conditions simulation (Fig. 5, top panels) are virtually indistinguishable from the exact quantum simulations shown in the bottom panel. The spectrum converges very rapidly with respect to the number of the initial phase space points in the calculation. Note that one initial phase space point gives rise to $n_{t_1}\times n_{t_2}\times n_{t_3}=25\times 600\times 25$ slightly different classical trajectories. Aside from a higher level of noise, there is no noticeable difference between the 20 and the 400 trajectory simulations shown in Fig. 5. Interestingly, all semiclassical calculations have small spikes at the frequencies of the anti-Stokes transitions $[\omega_L-\omega_S=-(E_i-E_0)]$, this is the result of the incomplete representation of the ground vibrational state by the ensemble of initial conditions. When the number of initial phase points is increased the relative contribution of

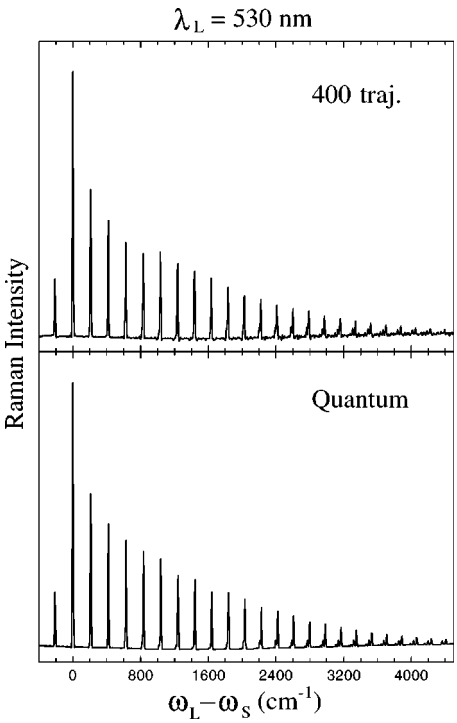

FIG. 6. Resonance Raman spectra of the one-dimensional system at $T=230$ K, computed with the semiclassical method (top panel) and the exact quantum mechanical result (bottom panel).

this artifact becomes smaller. In Fig. 6 we show the spectrum calculated at the temperature of 230 K (note the anti-Stokes line and anharmonic splittings at high overtones). Comparing the spectrum with the exact quantum result (bottom panel), once again, we find nearly exact agreement.

One more interesting feature of all the calculated spectra is the negative background observed in both the semiclassical and quantum results. This arises from the artificial partitioning of the total SLE spectrum into the R_1, R_2, and R_3 parts. If we perform the analytical double Fourier transform of Eq. (29) we find, besides the standard Raman expression, the two negative fluorescencelike terms that cancel out with the parts that correspond to R_1 and R_2 contributions. Since our time limits do not resolve the eigenstates of the B state, instead of the discrete lines a broad negative signal is observed.

The surprisingly good convergence of the spectra with the number of initial conditions encouraged us to look at the spectra generated from just a single point in phase space. In Fig. 7 we show the spectrum obtained from a single point $\mathbf{p}_0,\mathbf{q}_0$ selected randomly from the Husimi distribution at $T=0$. The result is very similar to the real spectrum. We notice that the spectrum is not purely real which means that the cancellation of complex parts is a result of quantum interference of trajectories originating at different points in phase space. The relative intensities are different from the converged spectrum, since they depend on the sampling of initial conditions in phase space. For example, a single trajectory spectrum always has a nonzero anti-Stokes contribution unless the initial conditions happen to coincide with the minimum energy point. Finally, we notice that in the single trajectory spectrum the spectral lines are spaced evenly, and

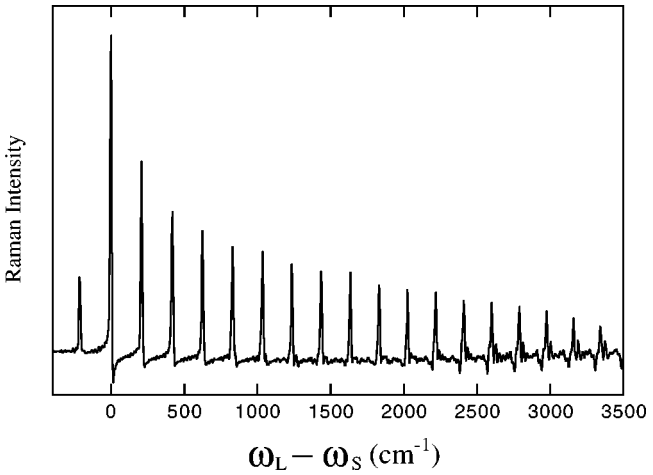

FIG. 7. Semiclassical RR spectrum obtained by sampling a single initial condition in the phase space.

carry no information about the anharmonicity of the ground state potential. Nevertheless, it is possible to use as a reference a spectrum generated from a single phase space point, i.e., given by a single term in the sum of Eq. (14). This language may be useful in discussing many-body systems, where such analysis can establish the correspondence between spectral features and the actual dynamics of the system (e.g., broadening of the particular lines and the corresponding interactions with the bath).

To examine the connection between the dynamics of an individual trajectory, its correlation function and its spectrum, let us look at a phase space portrait of a trajectory for $t_1=6$ fs, $t_2=1200$ fs, and $t_3=6$ fs shown in Fig. 8. The circular orbits correspond to the propagation of trajectory forward for time interval $+t_2$ (small circle) and backward for the interval $-t_2-t_3$ (large circle) on the ground state PES. The long, nearly vertical, lines are the result of propagation on the excited PES for $+t_3$, and for $-t_1$ time intervals. The correlation function is large when the overlap between the final and initial position is large. In the picture we have drawn circles around the initial and final positions that represent the coherent states. The times have been selected so that the overlap is high. This means that the propagations on the excited state forward must roughly cancel the propagation on the excited state backward in time. Thus we conclude that the correlation is the largest when $t_1 \approx t_3$, and the propagation on the larger circle for time t_2 consists of whole number of vibrations. The latter can be verified by plotting the response function $R_3(t',t,t')$ vs t at a given t' as it is done in Fig. 9. Here the plot is the result of an ensemble of 400 trajectories, which leads to the broadening of the correlation recurrences due to the anharmonicity of the system.

If we rewrite the expression of Eq. (1) for the spectrum as

$$I_{\mathrm{Raman}}(\omega_L,\omega_S)=2\,\mathrm{Re}\int_0^\infty dt_3\int_0^\infty dt_2\int_0^\infty dt_1 e^{i[(\omega_L+\omega_S)/2](t_1-t_3)} \times e^{i(\omega_L-\omega_S)(t_2+[(t_1+t_3)/2])}R_3(t_1,t_2,t_3) \quad (31)$$

we can better understand the physics projected by the Fourier

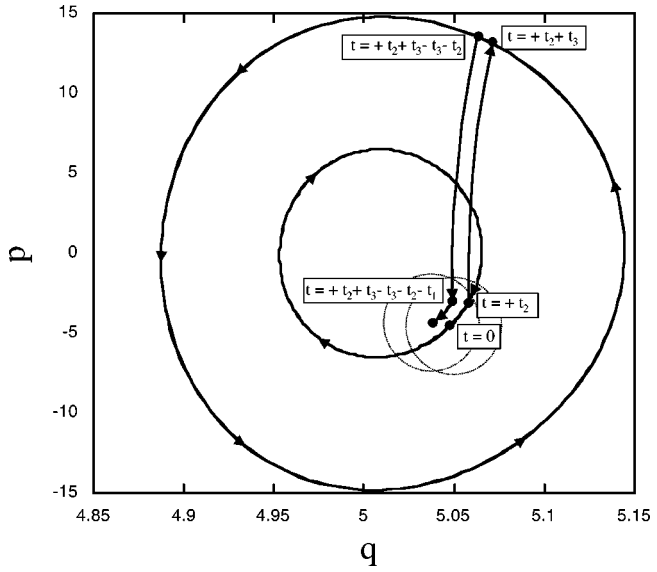

FIG. 8. Phase space portrait of the trajectory that enters into the semiclassical evaluation of the nonlinear response function. Both momenta and coordinates are plotted in a.u.

filters. The second exponential in Eq. (31) filters the frequencies that correspond to the differences in the action S_{+t-t} that result from the difference in the motion on large and small circles in opposite directions. The overtone that corresponds to a trajectory is given by the phase space volume located between the large and the small circle as given by the Born–Sommerfeld quantization rules. In the example shown in Fig. 8, the trajectory roughly corresponds to the fifth overtone. Large t_1 and t_3 lead to high displacement between the circles, thus they are mainly responsible for the high RR overtones, while the small t_1 and t_3 result in the backward propagation being very close to the forward propagation and mainly contribute to the Raleigh line ($\omega_L=\omega_S$) and the nearest RR lines. The first exponential simply makes sure that the laser light is in resonance with the energy difference between the two electronic states.

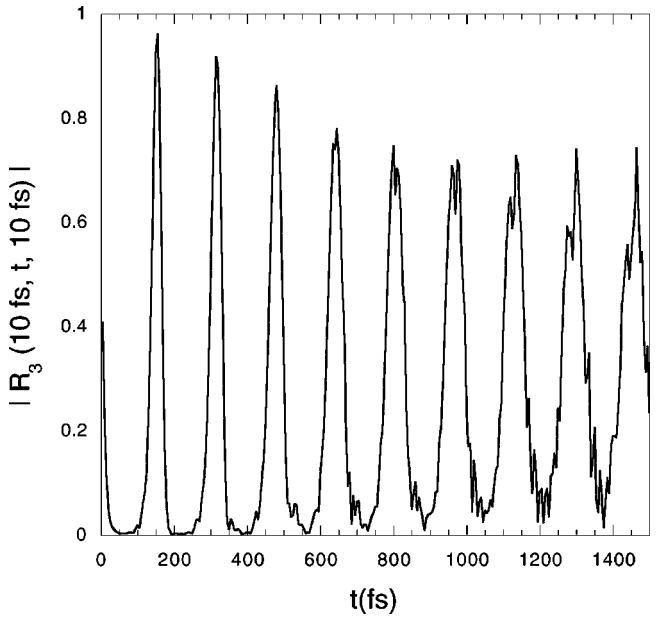

FIG. 9. The nonlinear response function $R_3(t_1,t_2,t_3)$ as a function the time t_2 at fixed $t_1=t_3=10$ fs for the one-dimensional system.

Let us now turn our attention to the correlation function itself and its convergence with respect to the number of trajectories. An important property of the correlation functions is their proper limit when the times t_1 or t_3 are equal to zero. If either of those times is zero the forward and backward propagators on time t_2 cancel each other and we obtain the simple result,

$$R_3(0,t_2,t)=C(t), \tag{32}$$

$$R_3(t,t_2,0)=C^*(t), \tag{33}$$

where $C(t)$ is the linear response correlation function in Eq. (13). The property in Eq. (33) is a numerical identity in our semiclassical evaluation. Indeed, if we consider the diagram in Fig. 4 with the zero time loop at its right end, the classical forward and backward propagation on t_2 exactly cancel each other, and we end up with the simple semiclassical evaluation of the function $C(t)$. The identity in Eq. (33) holds for each individual initial phase space point. However, the property in Eq. (32) is not satisfied for an individual initial condition. In the case of $t_1=0$, the left side loop of the diagram Fig. 4 is collapsed; this, however, does not result in the cancellation of backward propagation on the t_2 interval. Since the dynamics is nonlinear the divergence of initial and final position grows with t_2 for a given time interval t_3. The HK prefactor somewhat corrects for this effect; however, this correction is by no means an identity so this property becomes satisfied (or approximately satisfied, since the semiclassical expression is not exact) only as a result of an interference in an ensemble. This property is quite valuable since Eq. (32) can be used as a measure of convergence of the calculation. In Fig. 10 we plot the functions $R_3(0,t_2,t)$ vs t_2 at $t=1$, 3, 10 fs. The solid lines on the right represent the exact result given by $C(t)$, the thick lines represent the result of a 400 initial condition calculation, the thin lines underneath are the result of the 20 initial condition run. By examining these plots we can observe the loss of convergence with increasing times t_2 and t.

VI. MANY-BODY CALCULATIONS

In the present calculation the simplest model will be used for the I_2 in liquid Xe. The same Lennard-Jones potentials are used for the Xe–Xe atom–atom interactions and Xe–I interactions and are given by the parameters $\epsilon=282$ K and $\sigma=3.89$ Å. The I_2 X and B potentials are taken to be the Morse functions as used in the one-dimensional example. It was found that the smallest model that resembles a fluid must include at least a total of 12 atoms under periodic boundary conditions. A lower number of atoms leads to a significant reduction in the binding energy since the atoms do not have a full set of nearest neighbors. The simulation box size was initially chosen to be 10.2 Å, which corresponds to the density of liquid Xe at 230 K, and then it was adjusted to be 9.5 Å in order to roughly bring the overall pressure to zero. The pressure was evaluated by classical MC simulations. Simple MD trajectories at 230 K showed that

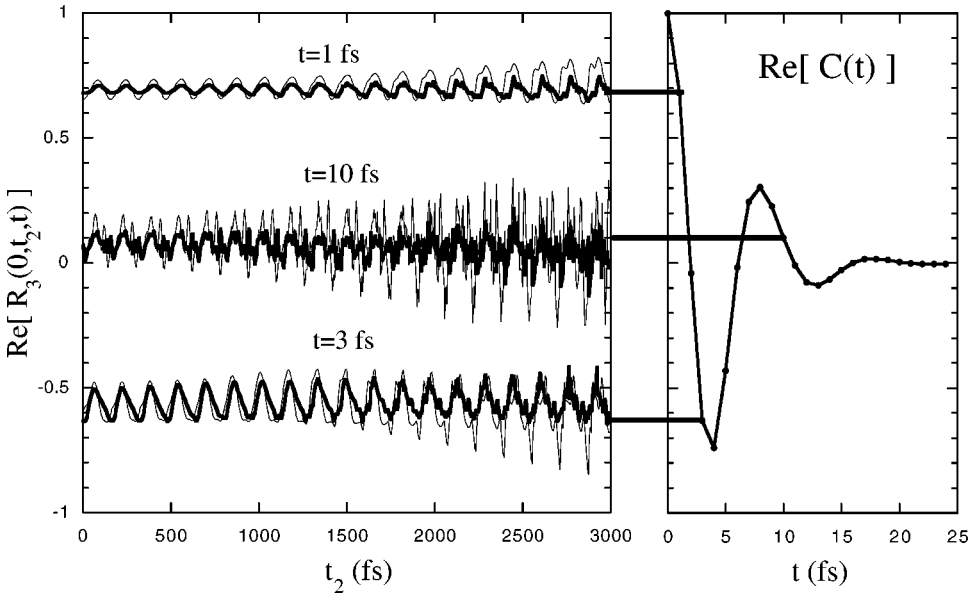

FIG. 10. The nonlinear response function $R_3(t_1,t_2,t)$ as a function the time t_2 at fixed $t_1=0;t=1,3,10$ fs for the one-dimensional system compared to the values given by the linear correlation function $C(t)$.

indeed the system shows liquidlike behavior with Xe atoms diffusing across the box on the time scale of several picoseconds.

All the calculations were done in the Cartesian coordinates of the atoms. The matrix γ was chosen to be diagonal, with the diagonal elements corresponding to a frequency 60 cm^{-1} in every degree of freedom. This choice is arbitrary; however in our unit system it satisfies both criteria $kT \gtrsim \gamma_{ii}$ and that the local harmonic nature of the potential is insured over the width of the Gaussian. This choice was tested by performing the similar calculation for the correlation function R_3 with the $\gamma_{ii}=120$ cm^{-1} which verified that results do not depend on this parameter. The overall convergence of the semiclassical method does not depend significantly on this parameter as well. The correlation function R_3 was calculated for the times $t_1,t_3=0,1,2,\ldots,19$ fs, $t_2=0,5,10,\ldots,1800$ fs.

The spectra at various laser frequencies ω_L generated from the response function at $T=230$ K are shown in Fig. 11. The response function R_3 was obtained by running a total of 288 trajectories. The overall appearance of the spectrum is quite similar to the experimental one aside from the broad background (see Fig. 1). Clearly the broadening of the vibrational overtones grows with overtone number. A complete numerical comparison is somewhat difficult due to the noise in both the experiment and simulation. However, several observations can be made. The width of the overtones 1–4 in the experimental spectrum are limited by the instrumental resolution. For the overtones 7–8, both the experimental and calculated FWHM are 80 ± 10 cm^{-1}. The widths of the overtones 11 and higher become larger than the spacing between the overtones both in experiment and simulation.

We can analyze the convergence of our results in two different ways. First is the standard criterion of convergence — independence of the spectrum on the number of trajectories. As in the one-dimensional case it was found that the spectrum converges very rapidly: a 40 trajectory run gives a spectrum that is nearly the same as that shown in Fig. 11. The other convergence criterion is the property of the response function R_3 in Eq. (32). In Fig. 12 we show the response function $R_3(0,t,t_3)$ for $t_3=1$ and 5 fs and compare that to the straight lines given by the known behavior $C(t_3)$. For $t_3=1$ fs, the property in Eq. (32) is roughly satisfied over the whole range of time. For higher times ($t_3 \gtrsim 4$ fs),

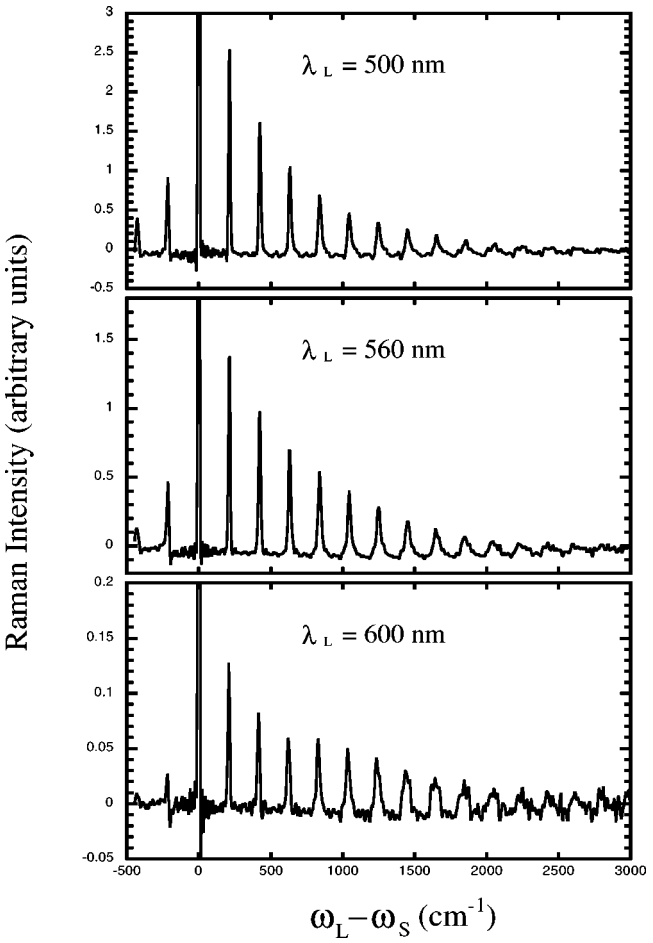

FIG. 11. Resonance Raman spectra computed for different excitation wavelengths for the I_2Xe_{10} system.

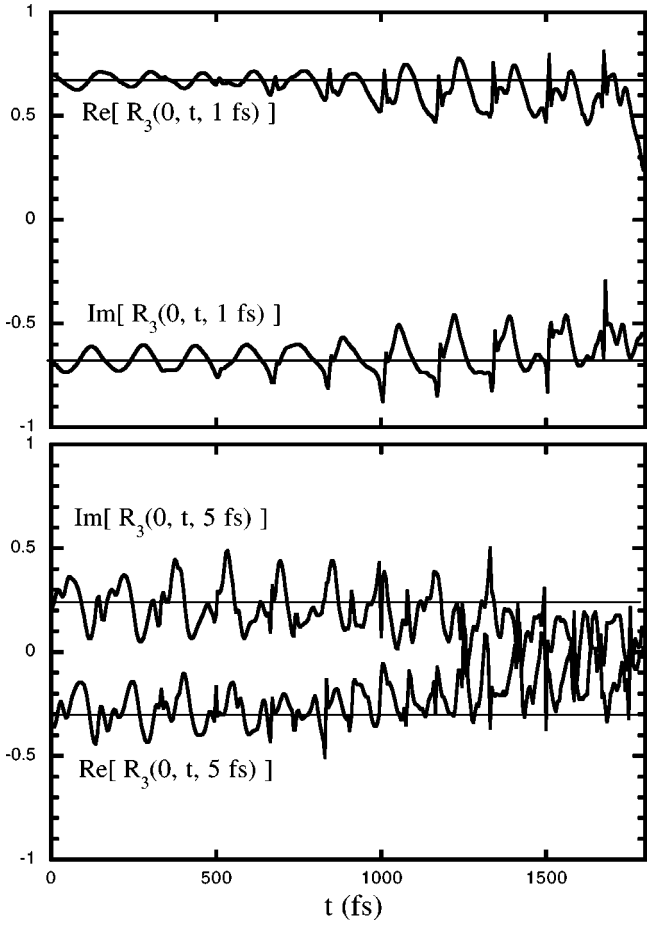

FIG. 12. The nonlinear response function $R_3(t_1,t_2,t_3)$ as a function the time t_2 at fixed $t_1=0;t_3=1,5$ fs for the I_2Xe_{10} system compared to the values given by the linear correlation function $C(t)$.

however, we find that the response function starts to deviate from the straight lines starting at about $t=1000$ fs. We have not observed any dependence of this deviation on the size of the calculation in the range between 40 and 288 trajectories. This deviation can be interpreted in two different ways. First, it is possible that the actual accuracy of HK propagator (7) is not sufficient to satisfy (32) at t above 1000 fs. Second, we may not have the full convergence with respect to the number of trajectories at $t>1000$ fs. It is possible that the significant contributions to this particular slice of the response function at high t is given by the rare initial conditions that are not being sampled at the numbers of trajectories that we can afford. In either case the correlation function seems to be converged at $t<1000$ fs, which validates most of our results.

Let us now analyze the broadening of the overtones. In Fig. 13 the response functions $R(t',t,t')$ are plotted and a higher rate of decay with t is clearly observed, the higher are the times t'. This analysis leads to another interesting observation: the Raleigh line must have an infinitely sharp component even in systems with significant dephasing since $R_3(0,t_2,0)\equiv 1$.

Two mechanisms can be proposed for the broadening of the overtones. The first is the homogeneous broadening, which is the result of the interaction of the I_2 motion with the solvent degrees of freedom. The second is the inhomogeneous broadening that results from the spread of the vibrational frequencies of I_2 depending on the solvent configuration. The single trajectory calculations shown in Fig. 14 show that the broadening for an individual trajectory is typically smaller than the one observed in the overall spectrum which points to the second mechanism.

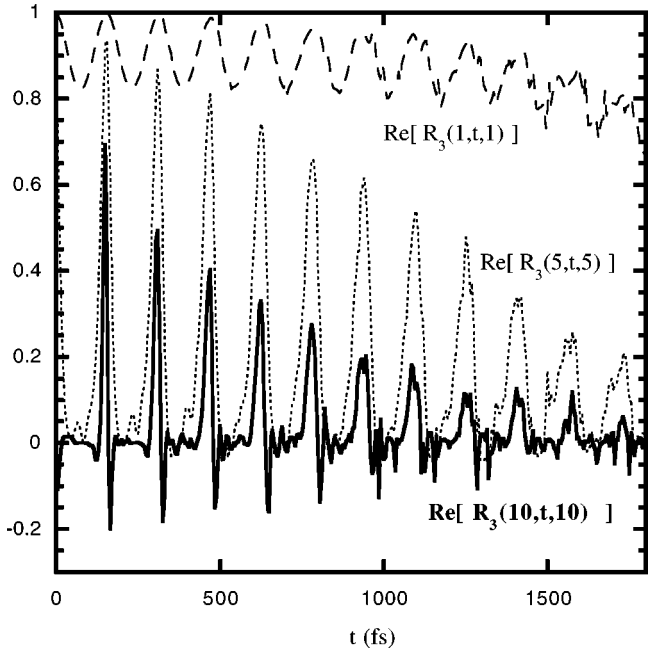

FIG. 13. The nonlinear response function $R_3(t_1,t_2,t_3)$ as a function the time t_2 at fixed $t_1=t_3=1,5,10$ fs. for the I_2Xe_{10} system.

The efficiency of the method, i.e., the small numbers of initial conditions at which the spectrum is converged seems impressive. It is even more remarkable if we note that at the end of the forward propagation for 1800 fs the average absolute value of the pre-exponential factor is $\langle|J_{+t}|\rangle\sim 10^8$. This extreme growth of the prefactor is caused by the nonlinear dynamics of the liquid. However, most of this dynamics cancels out during the backward propagation to end up

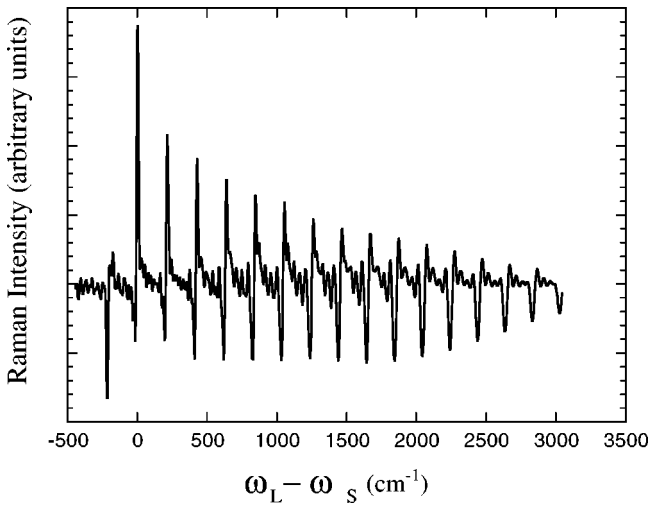

FIG. 14. RR spectrum of I_2Xe_{10} obtained by sampling a single initial condition in the phase space.

with very small prefactors at the end of the loop $\langle|J_{+t-t}|\rangle \sim 1.1-10$. This observation suggests that for most solvent degrees of freedom the monodromy matrix at the end of the loop is exactly unity; thus, for these degrees of freedom, it may not be necessary to evaluate the monodromy matrix at all, which, for a large system, could mean a significant gain in efficiency. A modified method along those lines, which we propose for future investigation, would include two steps: (1) a single test trajectory is propagated to determine the subset of degrees of freedom that interact with the electronic transition at given initial conditions; (2) in the computations following from these initial conditions the monodromy matrix is computed only for the subspace found in step (1). The present calculation took about one week on 48 Pentium II nodes of an Intel cluster. Application of the method to a larger system might require the implementation of the above approximation to avoid an N^3 scaling in the calculation of the dynamics.

VII. CONCLUSIONS

In this work, a practical method for the semiclassical calculation of multiple-time quantum correlation functions in systems of large dimensionality has been demonstrated. The method combines: (1) HK semiclassical propagation; (2) FB evaluation of trajectories over time-circuits; and (3) a new expression for the thermal density matrix in the representation of coherent states. The full second-order semiclassical MD has been computed for the 36-dimensional system with realistic pair potentials as sole input. We note that dynamics of a 40-dimensional system with a model PES has been recently calculated by Miller and co-workers.[18]

To our knowledge, this is the first work in which the three-time nonlinear response function is computed directly from the molecular dynamics of a complex system. Here we have specialized the application to RR spectra in condensed phase.[34] It should be recognized, however, that three-time correlation functions describe the whole family of coherent four-wave mixing spectroscopies, such as CARS and photon echo.[2] Thus, this work opens up the door to direct MD interpretation of the large volume of modern experiments in the field of femtosecond nonlinear spectroscopies.[35,36] The application of time-circuit diagrams to the analysis of time-resolved CARS experiments in condensed phase[37] and gas phase experiments involving large rovibrational superpositions,[38] has recently been illustrated. Finally, we should note that time correlation functions that describe quantum evolution over optically coupled electronic states are also appropriate for describing nonadiabatic dynamics over multiple electronic states with various couplings.

ACKNOWLEDGMENTS

Dr. Mark Brewer has helped at all stages of the work, and we thank him for important discussions on the semiclassical methods, help with the exact quantum mechanical calculations, and valuable comments on the manuscript. We would also like to thank Professor David Tannor for numerous discussions on the subject of nonlinear response functions during his stay at UC Irvine. The research has been funded in parts by National Science Foundation Grant Nos. CHE-9712884 and CHE-9708382, and by the University of Utah Center for the Simulation of Accidental Fires and Explosions (C-SAFE), funded by the Department of Energy, Lawrence Livermore National Laboratory, under Subcontract No. B841493.

[1] E. J. Heller, Acc. Chem. Res. **14**, 368 (1981).
[2] S. Mukamel, *Principles of Nonlinear Optical Spectroscopy* (Oxford University Press, New York, 1995).
[3] W. H. Miller, J. Chem. Phys. **53**, 3578 (1970).
[4] M. F. Herman and E. Kluk, Chem. Phys. **91**, 27 (1984); E. Kluk, M. F. Herman, and H. L. Davis, J. Chem. Phys. **84**, 326 (1986); M. F. Herman, *ibid.* **85**, 2069 (1986).
[5] K. G. Kay, J. Chem. Phys. **100**, 4377 (1994); **100**, 4432 (1994); **101**, 2250 (1994).
[6] J. Cao and G. A. Voth, J. Chem. Phys. **104**, 273 (1996).
[7] A. R. Walton and D. E. Manolopoulos, Chem. Phys. Lett. **244**, 448 (1995); Mol. Phys. **87**, 916 (1997).
[8] M. L. Brewer, J. S. Hulme, and D. E. Manolopoulos, J. Chem. Phys. **106**, 5775 (1997).
[9] M. Ovchinnikov and V. A. Apkarian, J. Chem. Phys. **108**, 2277 (1998).
[10] S. Garashchuk and D. Tannor, Chem. Phys. Lett. **262**, 477 (1996); S. Garashchuk, F. Grossmann, and D. Tannor, J. Chem. Soc., Faraday Trans. **93**, 781 (1997).
[11] F. Grossmann and E. J. Heller, Chem. Phys. Lett. **241**, 45 (1995); M. A. Sepulveda and F. Grossmann, Adv. Chem. Phys. **96**, 191 (1996).
[12] V. A. Mandelshtam and M. Ovchinnikov, J. Chem. Phys. **108**, 9206 (1998).
[13] B. W. Spath and W. H. Miller, J. Chem. Phys. **104**, 95 (1996).
[14] X. Sun and W. H. Miller, J. Chem. Phys. **108**, 8870 (1998).
[15] V. S. Batista and W. H. Miller, J. Chem. Phys. **108**, 498 (1998).
[16] V. S. Batista, M. T. Zanni, B. J. Greenblatt, D. M. Newmark, and W. H. Miller, J. Chem. Phys. **110**, 3736 (1999).
[17] K. Thompson and N. Makri, Phys. Rev. E **59**, 4729 (1999); N. Makri and K. Thompson, Chem. Phys. Lett. **291**, 101 (1998).
[18] X. Sun and W. H. Miller, J. Chem. Phys. **110**, 6635 (1999); H. Wang, M. Thoss, and W. H. Miller, *ibid.* **112**, 47 (2000).
[19] O. Kühn and N. Makri, J. Phys. Chem. **103**, 9487 (1999).
[20] S. Y. Lee and E. J. Heller, J. Chem. Phys. **71**, 4777 (1979).
[21] A. B. Myers, J. Opt. Soc. Am. B **7**, 1665 (1990).
[22] J. Almy, K. Kizer, R. Zadoyan, and V. A. Apkarian, J. Phys. Chem. A **104**, 3508 (2000).
[23] W. F. Howard and L. Andrews, J. Raman Spectrosc. **2**, 442 (1974); J. Graybowski and L. Andrews, *ibid.* **4**, 99 (1975); L. Andrews, Appl. Spectrosc. Rev. **11**, 125 (1976).
[24] R. J. Sension and H. L. Strauss, J. Chem. Phys. **85**, 3791 (1986); R. J. Sension, T. Kobayashi, and H. L. Strauss, *ibid.* **87**, 6221 (1987); R. J. Sension and H. L. Strauss, *ibid.* **88**, 2289 (1988).
[25] J. Xu, N. Schwnetner, and M. Chergui, J. Chem. Phys. **101**, 7381 (1994); J. Xu, N. Schwnetner, S. Hennig, and M. Chergui, J. Raman Spectrosc. **28**, 433 (1997).
[26] In their analysis of SLE of I_2 in rare gas solids, Almy *et al.* (Ref. 22) suggest that this emission must occur at the same time scale as the RR progression, and therefore suggest that the sharp and broad SLE contributions originate from ''T''-shaped and linear I_2:Xe configurations in the liquid.
[27] P. Jungwirth and R. B. Gerber, J. Chem. Phys. **102**, 8855 (1995); P. Jungwirth, E. Fredj, and R. B. Gerber, *ibid.* **104**, 9332 (1996).
[28] M. Ovchinnikov and V. A. Apkarian, J. Chem. Phys. **105**, 10312 (1996); **106**, 5775 (1997).
[29] R. G. Gordon, Adv. Magn. Reson. **3**, 1 (1968).
[30] M. L. Brewer, J. Chem. Phys. **111**, 6168 (1999).
[31] M. Ovchinnikov and V. A. Apkarian, Proc. SPIE **3273**, 285 (1998).
[32] R. P. Feynman and A. R. Hibbs, *Quantum Mechanics and Path Integrals* (McGraw–Hill, New York, 1965).
[33] D. T. Colbert and W. H. Miller, J. Chem. Phys. **96**, 1982 (1992).
[34] A. E. Johnson and A. B. Myers, J. Phys. Chem. **100**, 7778 (1996).
[35] A. Tokmakoff, M. J. Lang, D. S. Larsen, G. R. Fleming, V. Chernyak, and S. Mukamel, Phys. Rev. Lett. **79**, 2702 (1997); A. Tokmakoff, M. J. Lang,

D. S. Larsen, and G. R. Fleming, Chem. Phys. Lett. **272**, 48 (1997); A. Tokmakoff and G. R. Fleming, J. Chem. Phys. **106**, 2569 (1997).
[36] See, for example, M. Cho, in *Advances in Multi-Photon Processes and Spectroscopy*, 1st ed., edited by S. H. Lin, A. A. Villaeys, and Y. Fujimura (World Scientific, Singapore, 1999), Vol. 12.
[37] M. Karavitis, R. Zadoyan, and V. A. Apkarian, J. Chem. Phys. **114**, 4131 (2001).
[38] R. Zadoyan and V. A. Apkarian, Chem. Phys. Lett. **326**, 1 (2000).